Bridge piers in mobile beds: visualization and characterization of the surrounding and approaching flows

Helena I.S. Nogueira
Instituto Superior Técnico, Lisboa

Mário J.R.P. Franca
Faculdade de Ciências e Tecnologia da Universidade de Coimbra, Coimbra

Rui M.L. Ferreira
Instituto Superior Técnico, Lisboa

ABSTRACT: A cylindrical obstacle intercepting the full depth of an open-channel flow changes the pressure field in its vincinity. In the upstream side of the cilinder, the adverse pressure gradient originates separation of the down-flow in front of the cylinder and near its base. The separated flow is organised in a system of vortexes, dominated by a horseshoe vortex. The general objective of this work is to characterize the turbulent separated flow dominated by the horseshoe vortex in front of the cylinder in several locations along a developing turbulent boundary layer. It is also intended to characterize the flow in a scour hole, namely the downflow, the horshoe vortex system and the separation vortex. The flow field is characterized in terms of mean velocities, Reynolds stresses, vorticity and streamlines. The raw data necessary to compute these quantities is essentially composed of instantaneous velocity fields obtained with Particle Image Velocimetry (PIV). It is shown that the intensity of the equivalent horseshoe vortex, defined as the vortex calculated for the mean velocity field, does not shows an evident variation with the Reynolds number based on the boundary layer thickness. Previously unreported results concerning the maximum size of the horseshoe vortex are presented and discussed. The intermittent nature of the main vortex is discussed and related with the occurrence of organised turbulent bursting structures. The relevance of the system of vortexes for the initiation of local scour is also discussed.

Keywords: Horseshoe vortex, Local scour, Turbulent flow, Developing boundary layer, PIV

1 INTRODUCTION

Enforcing the structural integrity of bridges requires the capacity to predict pier local scour morphology. The complex nature of the interaction between turbulent flow hydrodynamics, local morphology and sediment transport in the near field of the pier justifies the important volume of research performed on these topics. The contribution of the present work is mostly in the characterization of the turbulent flow in front of a bridge pier, idealised as a wall-mounted cylinder of vertical axis, intercepting the full depth of an open-channel flow with a developing boundary layer. Such a cylinder changes the pressure field around it. The adverse pressure gradient upstream the cylinder modifies the pattern of the approach flow, which becomes downward in the upstream face of the obstacle, while the remaining flow goes around the cylinder in the downstream direction (Morton 1987, Raudkivi 1998). If the pressure grandient becomes sufficiently strong, the interaction between the downward and the approaching flow results in flow separation near the base of the cylinder, where it develops, in a turbulent flow, a complex and unsteady vortex system known as the horseshoe vortex. If the cylinder is placed in mobile bed, upon reaching a certain flow velocity, the sediment particles close to the cylinder begin to move, leading to the formation of the scour hole.

The present work is aimed at the visualization and characterization of the down-flow and of the turbulent flow field in the separated region in front of the cylinder. The specific objectives are: i) to assess qualitatively and quantitatively the geometry and the intensity of the horseshoe vortex as a function of the boundary layer Reynolds number and ii) to characterise the down-flow and the vortex system inside a scour hole in its early stages of development in order to identify the most relevant scour mechanisms.

The work was essentially laboratorial and involved the use of Particle Image Velocimetry (PIV) for the visualization and quantification of the velocity field. Experiments were carried out to characterize: a) the time-averaged approaching flow,

defined as the flow upstream the pier but not affected by it, which, in a horizontal bed, is gradually accelerated and b) the turbulent horseshoe vortex and its interaction with the turbulent flow in the bed boundary layer and with the down-flow in front of the cylinder. Velocity measurements were performed in the vertical plane of symmetry in front of the cylinder and in vertical planes at 30º and 45º from the symmetry plane and in horizontal planes were also performed, only on selected experiments.

The main theoretical issues of this work are presented in section 2, as well as a short description of the latest works concerning the flow pattern around a cylinder. The experimental facilities are described in section 3 and the experimental procedure carried out is presented in section 4. The main results of the present work are presented and discussed in section 5, being section 6 devoted to conclusions.

2 STATE-OF-THE-ART REVIEW

A brief review of some of the most relevant studies of flow hydrodynamics in front of wall mounted cylindrical obstacles is presented. Since, in the present laboratorial work, the approaching flow was gradually varied, the formulas for the Reynolds stresses and time-averaged longitudinal velocity profiles are also presented.

The velocity distribution in the inner region of a hydraulically transitional boundary layer can be approached by the log-law

$$\frac{u}{u_*} = \frac{1}{\kappa}\ln\left(\frac{z}{k_s}\right) + B \tag{1}$$

where z is the vertical coordinate, u_* is the friction velocity, k_s is the roughness length, $\kappa = 0.41$ is the von Kármán constant and B is a function of the bed Reynolds number ($\mathrm{Re}_* = u_* k_s / \nu$) and a function of the gradient of the flow depth, in gradually varied flows. The Reynolds stress profile is

$$\frac{\partial \tau}{\partial z} = g\rho^{(w)}\left(\frac{\partial h}{\partial x} + \frac{\partial z_0}{\partial x}\right) \tag{2}$$

where $\tau = -\rho^{(w)}\overline{u'w'}$ are the Reynolds stresses, u' and w' are the longitudinal and vertical instantaneous velocities, respectively, $\rho^{(w)}$ is the fluid density, h is the flow depth, z_0 is the bed elevation, g is the acceleration of gravity and x is the longitudinal coordinate.

In front of the cylinder, the separation area is characterized by a complex structure, eventually dominated by horseshoe vortex systems. Morton (1974) demonstrated that the vorticity mechanism is governed by the pressure field. The component of the vorticity normal to a vertical plane in the flow direction depends on the pressure gradient in the flow direction, as shown in equation (3):

$$\upsilon^{(w)}\partial_z \eta\big|_{z_0} = \frac{e_y}{\rho^{(w)}}\partial_x p \tag{3}$$

where $\upsilon^{(w)}$ is the fluid cinematic viscosity, η is the vorticity component in the transversal direction (y) and p is the total pressure.

The vorticity field is solenoidal. Hence, the vortex intensity, defined as

$$I_v = \int_\Omega \boldsymbol{\omega}\cdot n\, dA = \int_G \eta\, dA \tag{4}$$

is conserved in any section around the cylinder. The term $\boldsymbol{\omega}$ represents the vector of the vorticity.

Baker (1979, 1980, 1985) investigated the characteristics of the horseshoe vortex near a cylinder embedded in a horizontal fixed bed. For all flow conditions tested, he observed the existence of a horseshoe vortex system consisting of at least two vortices (Figure 1).

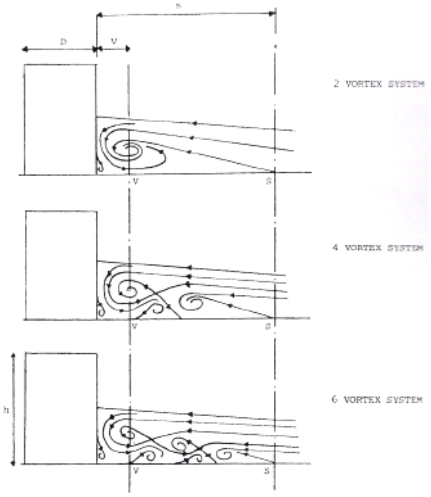

Figure 1. Horseshoe vortex system (adapted from Baker 1985).

Shen et al. (1969) studied the mechanism of local scour near cylindrical piers and suggest that the horseshoe vortex generated upstream the pier is due to the concentration of vorticity, induced by the obstacle, already existent in the flow field. They believe that this horseshoe vortex is the primary mechanism of local scour.

Qadar (1981) explored the interaction between horseshoe vortex and the temporal increase of scour depth. He proposed that the horseshoe vortex is approximated, in the symmetry plane, by a circle whose radius increases with the depth of the scour hole, as represented in Figure 2.

Muzzammil and Gangadhariah (2003) investigated the horseshoe vortex in the plane of symmetry through a visualisation technique that employs suspension of clay. They observed that the vortex shape is elliptical, instead of circular as defended by Qadar (1981). The dimensions of the horseshoe vortex were experimentally measured and

found to depend on the scour depth, diameter of the cylinder and Reynolds number. They pointed out the existence of a cusp and two distinct slopes in the scour hole, in the plane of symmetry, as shown in Figure 3.

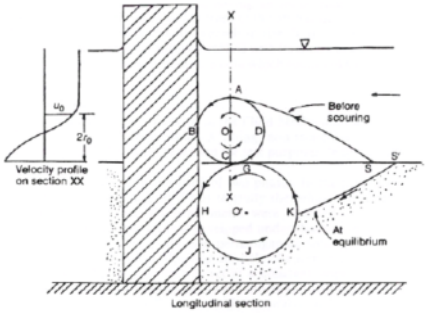

Figure 2. Evolution of the horseshoe vortex with the increase of the scour hole (adapted from Qadar 1981).

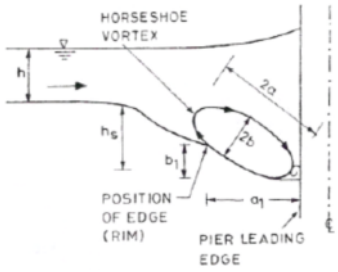

Figure 3. Scheme of horseshoe vortex upstream the cylinder in the scour hole (adapted from Muzzammil & Gangadhariah 2003).

Unger and Hager (2006) investigated the characteristics of the internal flow upstream a half-cylinder placed on the side wall of a channel. They performed a detailed temporal description of the horseshoe vortex with PIV. The placement of the cylinder at the lateral wall of the channel allows better visualization of the flow phenomena and a better quality of the data obtained. However, the turbulent boundary layer existent along the wall influences the flow behavior, so the results can not be directly compared with those obtained in the plane of symmetry of the channel.

They suggest that the equivalent vortex is located at the point of intersection of the two slopes in the scour hole, over the cusp (Figure 4), rather than located in the greater slope, as defendend by Muzzammil and Gangadhariah.

They conclude that the horseshoe vortex inside the continuously increasing scour hole and the downflow in front of the pier are the governing scour agents.

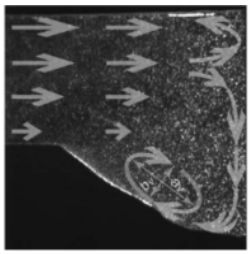

Figure 4. Schematic flow pattern inside the scour hole in front of the pier (adapted from Unger & Hager, 2007).

3 EXPERIMENTAL FACILITIES AND INSTRUMENTATION

The experiments were conducted in a 8,0 m long and 0,70 m wide rectangular flume (Figure 5). The water is recirculated from the reservoir (A) by means of a centrifugal pump (B). The water discharge was controlled by a flow meter (D) installed in the hydraulic circuit and the flow depth was controled by the adjustment of the downstream gate (F_2). A horizontal mobile bed reach 2,00 m long was placed 4,55 m downstream of the flume inlet (J and Figure 6a). In the upstream reach of the mobile bed, uniform quartz sand was glued on the flow bed, in order to increase its roughness. The bed material, used both on mobile and fixed bed, is characterized by a median diameter D_{50} of 0,837 mm and geometric standard deviation σ_D of 1,48.

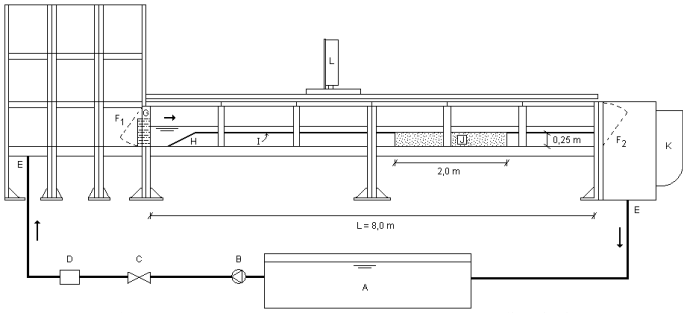

Figure 5. Experimental installation and hydraulic circuit.

The laser source was attached on a mobile carriage, settled on the rails of the channel (Figure 5L and Figure 6b). The PVC cylinder, of 0,48 m diameter, was placed in the symmetry axis of the channel (Figure 6c).

To investigate the effect of the roughness in the development of the turbulent boundary layer, velocity measurements on the approach flow were accomplished before and after the placement of granular material, 25 mm of characteristic diameter, in the upstream region of the flow bed. Figure 6d) shows the disposal of the rough elements in the flow bed.

The Particle Image Velocimetry (PIV) was used to measure the two-dimensional instantaneous

velocities of the flow. The double-pulsed Nd-YAG laser illuminates a given seccion of the flow which is recorded by a digital camera (Figure 7). The particles in the fluid scatter the light incident, which is detected by the camera, being further represented in frames as bright dots in a dark background, as shown in Figure 8a. The frames are then split in interrogation areas, being possible to calculate the displacement vector for each one of these areas, with help of correlation methods.

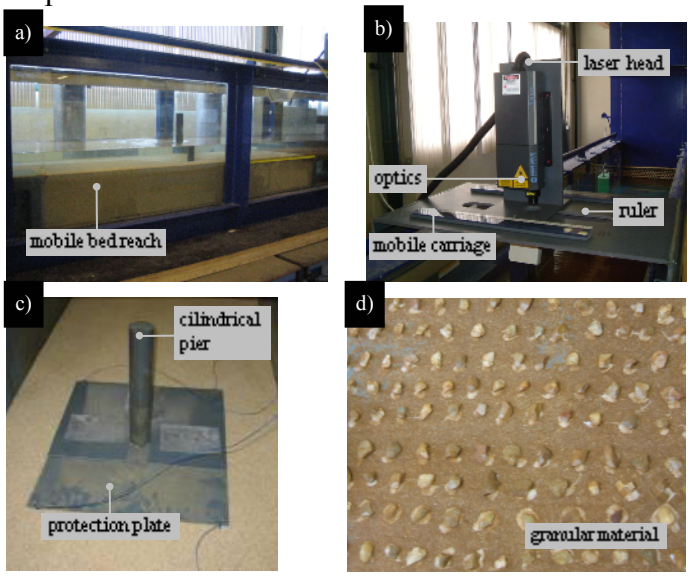

Figure 6. Additional elements to perform the velocity measurement tests. a) mobile bed reach; b) laser source; c) cylinder; d) disposal of the granular material.

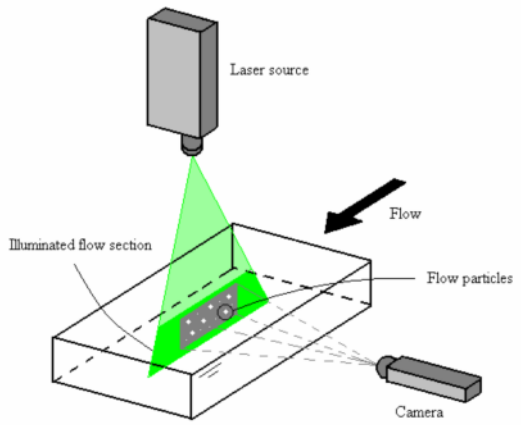

Figure 7. Schematic diagram of PIV measurements.

Using the time between image exposures, the displacement map is converted into instantaneous velocity map. Appling validation methods, non-coherent vectors are removed and substituted (Figure 8b and c), improving the obtained results.

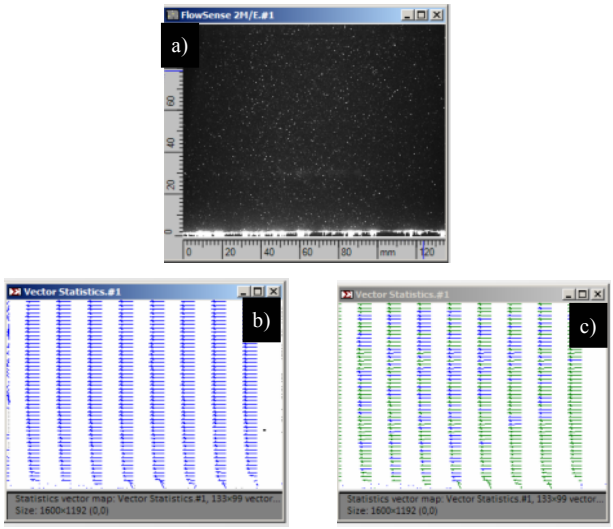

Figure 8 - Acquired image after laser exposure (a), averaged velocity maps, before (b) and after (c) the application of validation methods.

4 EXPERIMENTAL PROCEDURE

The velocity measurements were performed under clear water conditions, being the flow discharge established based on the concept of critical flow velocity. Three different criteria were used to estimate the value of critical velocity, being adopted the value $U_{cr} = 0{,}286\, m/s$ correspondent to the flow discharge of 20 l/s. Table 1 summarizes the flow variables and channel parameters of the experiments.

Table 1. Flow variables and channel parameters.

D_{50} (mm)	Q (m^3/s)	h (m)	U (m/s)	B/D (-)	B/h (-)
0,837	0,20	0,10	0,286	14,58	7,00

Velocity measurements were perferomed for six different vertical positions of the cylinder, as represented in Figure 9.

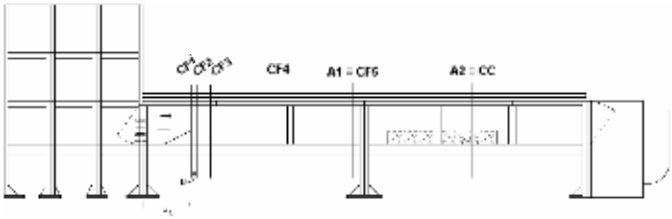

Figure 9. Representation of the different positions of the cylinder along the axis of symmetry of the channel.

The measurements on the approach flow were carried out at 4,40 and 6,0 m downstream the channel inlet, (tests A1 and A2, respectively, see Figure 9). Three different vertical planes were measured, as presentend in Figure 10, in order to investigate the lateral variation of the flow pattern.

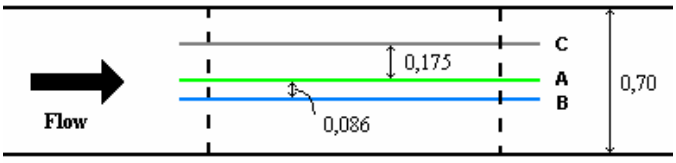

Figure 10. Representation of the sections of measurement. View from above. Dimensions in meters.

After the establishment of the flow conditions, the laser sheet is adjusted to illuminate the correct section of the flow. The next step is to focus the camera, with the help of a graduated object (Figure 11), and capture at least one frame for further calibration. The graduated object is removed from the flow and the parameters of the laser software are established to start the measurements.

The procedure for the characterization of the flow around the cylinder is similar to what was done for the approach flow. The cylinder was placed along the symmetry axis of the channel, in five different positions (tests CF1 to CF5, Figure 9). The cylinder placed in the flow field causes oscillation of the flow surface upstream the obstacle so, to inhibit optical problems with surface waves, the water surface was covered with an acetate sheet (Figure 11). Measurements were preformed upstream the cylinder in vertical planes in the symmetry axis, 30º from the symmetry axis (only in test CF5) and in horizotal planes 5 mm from the flow bed (in tests CF2 and CF5).

Figure 11. Additional material used in experiments. Left: graduated object; right: acetate sheet placed on the flow surface, downstream view.

The cylinder was placed in mobile bed (test CC) and for 5 minutes a scour hole developed around the obstacle (Figure 12, a). Subsequently, the sediment bed was fixed with spray varnish to prevent the movement of the bed material during the measurements. The tests were performed in a superficial region of the scour hole, in the symmetry axis and 30º from it, and inside the scour hole, 45º from the symmetry axis. Measurements in a horizontal plane, 5 mm from the bed, were also performed.

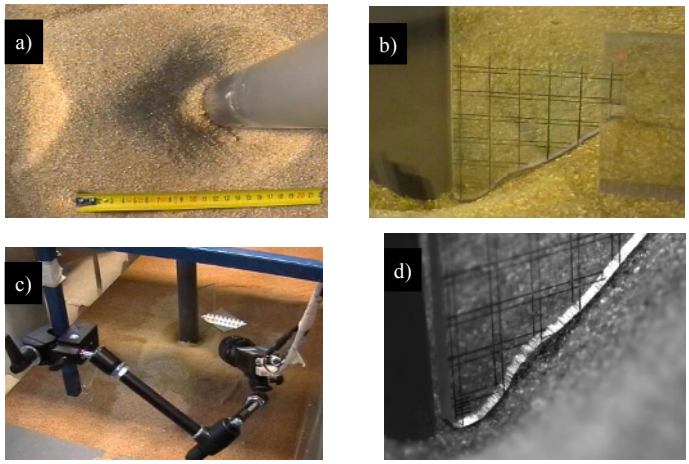

Figure 12. Measurements inside the scour hole. a) scour hole, downstream view; b) graduated object used for image calibration; c) arrangement of the measurement equipment; d) image acquired for calibration.

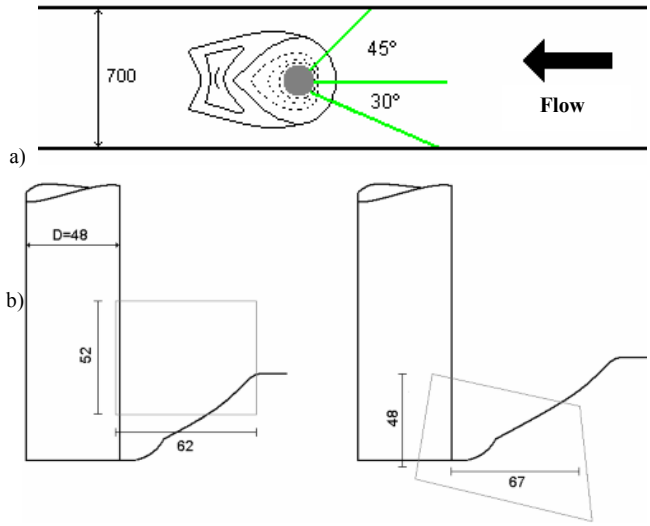

Figure 13 –Vertical measuring planes in the scour hole. a) view from above. Dashed line stands for negative values of bed topography, continuous line stands for positive values; b) side view: location of images and their dimensions. Left: vertical plane in the symmetry axis and at 30º; right: inside the scour hole, vertical plane at 45º from the symmetry axis. Dimensions in milimeters.

5 RESULTS AND DISCUSSION

5.1 *Gradually varied approaching flow*

The time-averaged velocity component u and Reynolds stress profiles obtained in the axis of symmetry of the approaching flow are presented in Figure 14. In subcritical regime, the flow over a horizontal bed is gradually accelerated and the pressure gradient is negative, which causes the Reynolds stress profile to become concave. The shear stress and the velocity profiles (Figure 14)

show that the boundary layer is not completely developed.

The friction velocity and constant B were obtained through the adjustment of the log-law equation (1) to the velocity profiles in the logaritmic sublayer (region delimited by the dashed lines in Figure 14, left). The characteristic roughness length k_s adopted was $2D_{50} \approx 1{,}50\,mm$ (Smart 1999). The friction velocity was also estimated from the Reynolds stress profile, for comparison. The results are shown in plots of Figure 14.

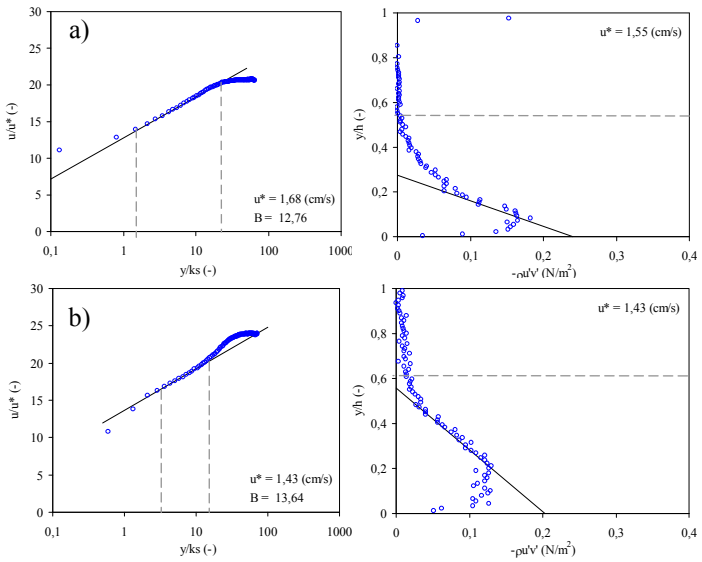

Figure 14. Vertical velocity (left) and Reynolds stress (right) profiles of the approaching flow. a) test A1; b) test A2; c) tests with granular material upstream. Test data (○) and theoretical approximations (–).

The values of B are higher than the mean values found in the literature (Schlichting, 1979). The differences may be due to an incorrect estimation of the roughness length and the incomplete development of the turbulent boundary layer.

5.2 *Flow upstream the cylinder in fixed bed*

The time-averaged velocity components u, v and w in the upstream face of the cylinder, in tests CF2 and CF5, are presented in Figure 15 and in Figure 16, respectively. The linear dimensions are normalized by the cylinder diameter D.

Before reaching the flow bed, the approaching flow is potential. The inclined inlet structure induces the development of an incipient boundary layer and flow acceleration, as shown by the distribution of the u-component. The negative values of the w-component near the flow bed indicates the existence of the down-flow. Further downstream, in test CF5 (Figure 16), the boundary layer is thicker and the magnitude of the w-component in the face of the cylinder is greater than the u-component. The transversal component is negligible in the symmetry axis, which means that the flow in this region is almost entirely downward.

The magnitude of the downflow is, thus, seen to depend on the development of the boundary layer and to increase with the flow depth.

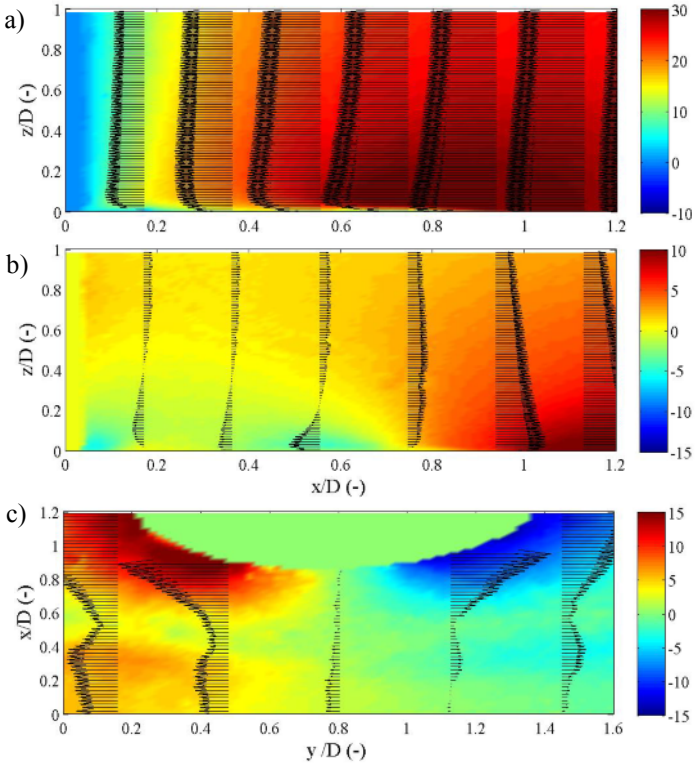

Figure 15. Time-averaged velocity components in test CF2. a) longitudinal component u; b) vertical component w; transversal component v. Velocities in cm/s.

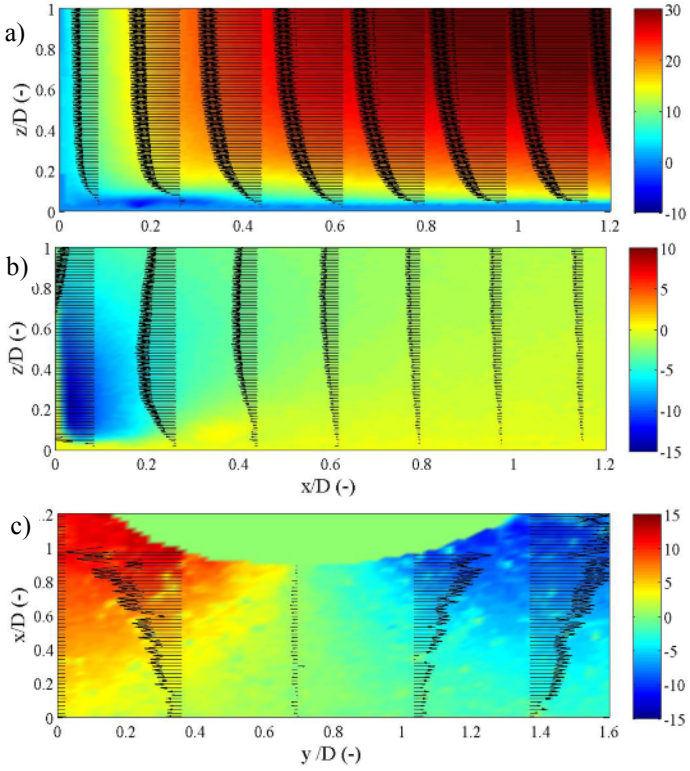

Figure 16. Time-averaged velocity components in test CF5. a) longitudinal component u; b) vertical component w; transversal component v. Velocities in cm/s.

The time-averaged vorticity maps and streamlines obtained in the measuring stations are presented in Figure 18. Figure 19 and 20 shows instantaneous vorticity maps.

The dimensions of the horseshoe vortex were estimated based on the vorticity maps, as shown in Figure 17, being the vortex diameter D_v determined by $D_V = \sqrt{ab}$.

This procedure was applied to the greatest instantaneous vortex observed in each test and to the equivelent vortex, wich is characterized by the separated flow region that shows a circulation pattern with non-zero vorticity and resulting from the time-averaged vortical instantaneous structures registred in that flow region.

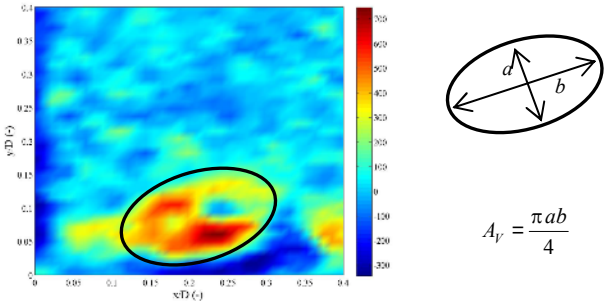

Figure 17. Dimensions of the horseshoe vortex.

When the cylinder intercepts the potential flow (test CF1), no horseshoe vortex was detected in the mean flow as well as no significant downflow. That is consistent with the theoretical result that links the horseshoe vortex with the concentration of vorticity already existent in a boundary layer (Morton 1987).

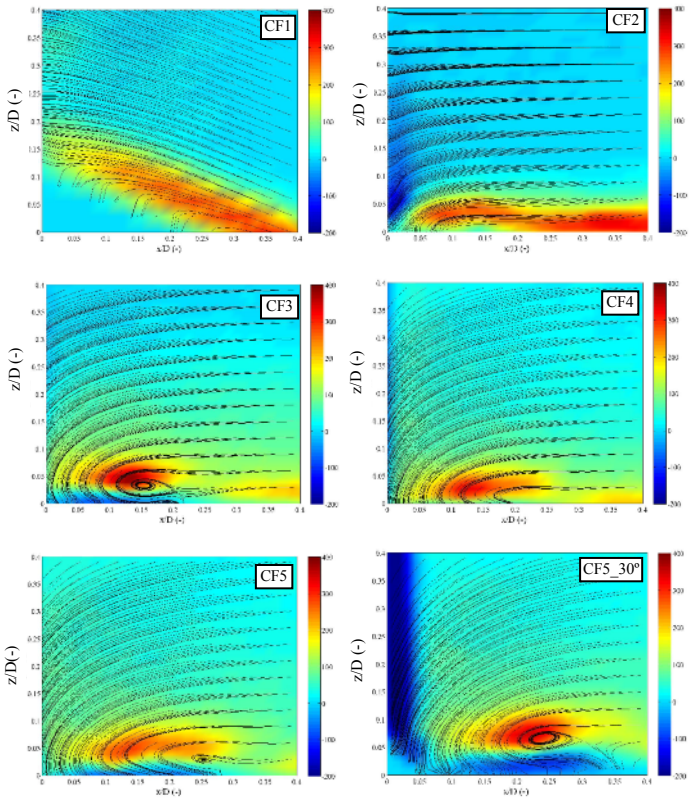

Figure 18. Time-averaged vorticity maps and streamlines.

In test CF2, the curvature of the streamlines near the base of the obstacle, associated with positive values of vorticity, suggests that the averaged flow pattern is downward, although no equivalent vortex is well defined. However, the instantaneous maps #19 and #190 shows the existence of well-defined intermittent vortexes. The gradients that are established in the velocity field lead to the stretch, and consequent decrease, of the vortex diameter, as well as the transportation and overlap of vorticity of opposite sign (Morton 1987). Locally, these effects lead to the annihilation of the vortex system.

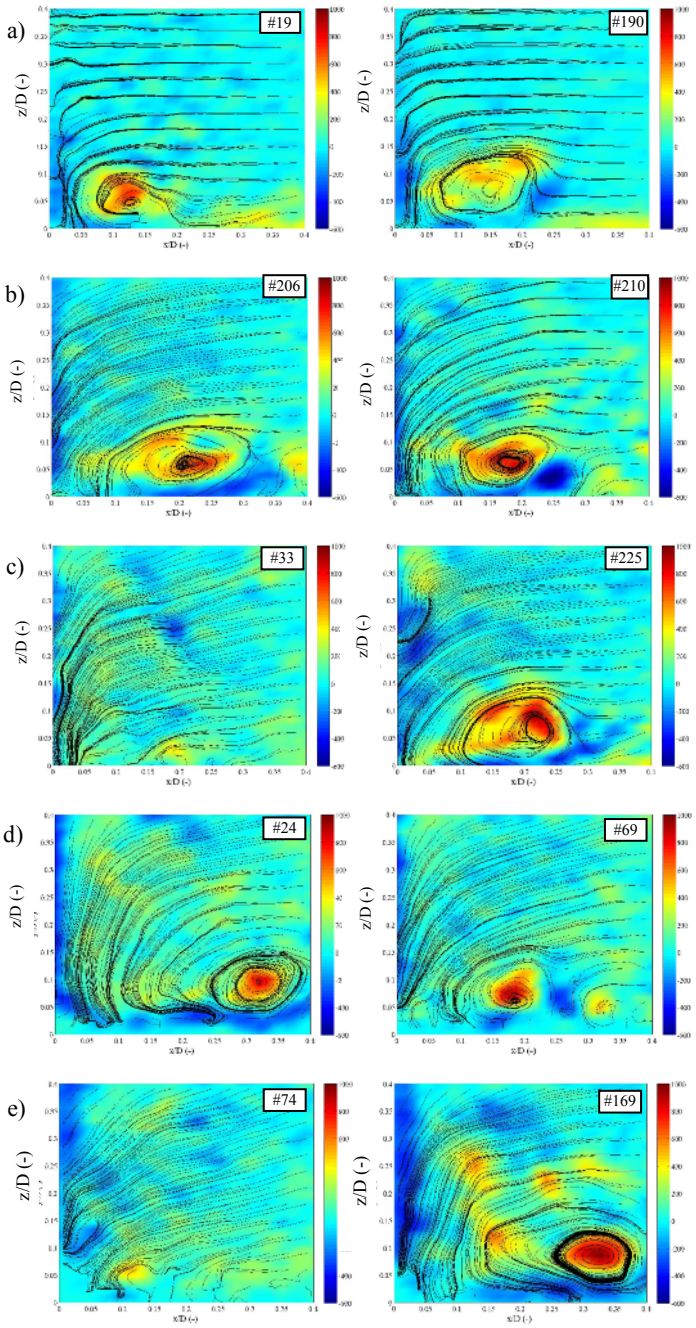

Figure 19. Instantaneous vorticity maps. a) test CF2; b) test CF3; c) test CF4; d) test CF5; e) test CF5, at a vertical plane 30º from the symmetry axis.

The time-averaged vorticity map of test CF3 shows the presence of an equivalent horseshoe vortex. Further downstream, the time-averaged vorticity maps show an increasing region of positive

vorticity near the flow bed and negative vorticity near the face of the cylinder. It is observed that the vortex location, relatively to the cylinder, depends on the boundary layer thickness. With an increasing thickness of the boundary layer, the longitudinal dispersion of the vortex location also increases.

The diameter of the equivalent vortex seems to increase with the thickness of the boundary layer. However, the instantaneous vortexes are apparently independent of the thickness of the boundary layer. These results summarized in Table 2 and in Figure 20a.

The intensity of the vortexes was also assessed. Its functional relation with the flow, sediment and geometrical variables reads

$$I_v = f\left(\mu^{(w)}, \delta, D, U, \rho^{(w)}, k_p, D_{50}\right) \qquad (5)$$

where I_v is the vortex intensity, $\mu^{(w)}$ and $\rho^{(w)}$ are the fluid viscosity and density, respectively, U is the depth-averaged mean velocity, D_{50} is the median diameter of the bed sediment and k_p is the surface roughness of the cylinder. Applying Vaschy-Buckingham thoerem to equation (5), one obtains

$$\frac{I_v}{UD} = f\left(\frac{UD}{\upsilon^{(w)}}, \frac{U\delta}{\upsilon^{(w)}}, \frac{k_p}{D}, \frac{D_{50}}{D}\right) \qquad (6)$$

where $UD/\upsilon^{(w)}$ reflects the effect of the cylinder diameter; $U\delta/\upsilon^{(w)}$ traduces the influence of the boundary layer thickness; k_p/D reflects the influence of the cylinder roughness; D/D_{50} traduces the bed roughness effect. It is noted that, in the present work, only the variation of I_v/UD with $Re_\delta = U\delta/\upsilon^{(w)}$ was assessed.

Table 2. Geometrical characteristics and intensity of mean flow and maximum instantaneous horseshoe vortexes.

Ensaio	d (mm)	a (mm)	b (mm)	A_v (mm^2)	D_v (mm)	w (s^{-1})	Iv (cm^2/s)	d/D (-)	D_v/D (-)	Ud/u (-)	I_v/UD (-)
CF1	0.0	0.0	0.0	0.0	0.0	0	0	0.00	0.00	0	0.00
CF2	2.0	0.0	0.0	0.0	0.0	0	0	0.04	0.00	578	0.00
CF3	8.1	2.4	6.7	12.7	4.0	290	37	0.17	0.08	2297	0.27
CF4	38.8	2.9	8.2	18.5	4.8	210	39	0.81	0.10	10976	0.28
CF5	62.4	2.4	9.6	18.1	4.8	208	38	1.30	0.10	17662	0.27
CF2_#190	2.0	5.8	7.2	32.6	6.4	280	91	0.04	0.13	578	0.66
CF3_#206	8.1	6.2	8.6	42.3	7.3	288	122	0.17	0.15	2297	0.89
CF4_#225	38.8	6.2	8.2	40.0	7.1	463	185	0.81	0.15	10976	1.35
CF5_#24	62.4	5.8	6.7	30.4	6.2	360	109	1.30	0.13	17662	0.80

Figure 20b (see also Table 2) shows the variation of I_v, computed from equation (4), with the boundary layer Reynolds number ($Re_\delta = U\delta/\upsilon^{(w)}$).
It is apparent that the mean flow vortex intensity is independent of the boundary layer Reynolds number. This is an indication that the most relevant variables for the geometry and the intensity of the mean-flow horseshoe vortex are the diameter of the cylinder and the flow velocity (Shen et al. 1969). As for the intensity of the maximum instantaneous vortex, the results shown in Figure 17b are inconclusive. An increasing trend is observed for lower boundary layer Reynolds numbers but the last data point does not confirm this trend.

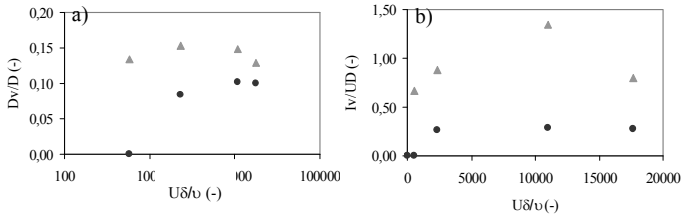

Figure 20. Dimensions of the horseshoe vortex as a function of the boundary layer thickness. (▲) maximim vortex in each measuring station; (●) equivalent vortex.

5.3 *Flow upstream the cylinder in the scour hole*

The time-averaged velocity components u and w obtained at the upper part of the scour hole are presented in Figure 21, in the symmetry axis, and in Figure 22, in a plane 30º from the symmetry axis (see also Figure 13). Figure 23 shows the velocity field inside the scour hole, in a vertical plane at 45º from the symmetry axis. In Figure 2, in the upstream region, it is noted the dominance of the u-component, being the vertical component pratically negligible. As the flow approaches the cylinder, the situation reverses: the longitudinal component of the velocity decreases, accompanied with sucessively increasing values of the vertical component. Flow separation is observed near the flow bed: the velocity profiles obtained at $0{,}4 \le x/D \le 1{,}0$ show negative values of the u-component and positive values of the vertical component, in opposition of the flow pattern in the upper layers, which indicates the existence of rotational flow in this region. Inside the scour hole, the flow pattern is similar to the previously observed, being quite clear the dominance of the downflow against the longitudinal, near the face of the cylinder.

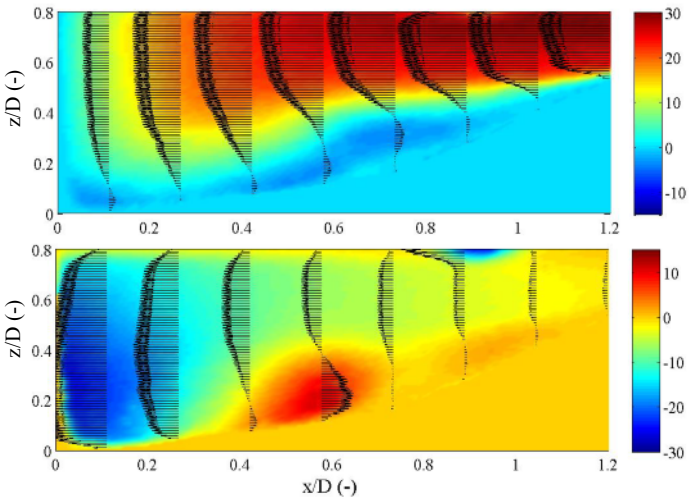

Figure 21 - Time-averaged velocity components in test CC, symmetry axis. On top: longitudinal component u; bottom: vertical component w. Velocities in cm/s.

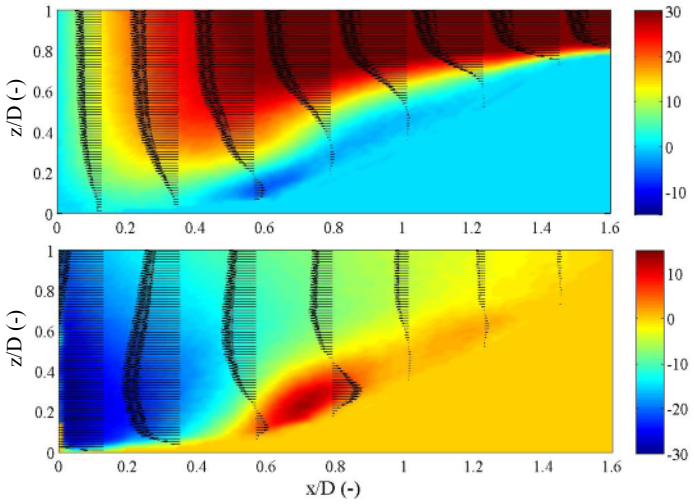

Figure 22 - Time-averaged velocity components in test CC, at 30º from the symmetry axis. On top: component u_p; bottom: vertical component w. Velocities in cm/s.

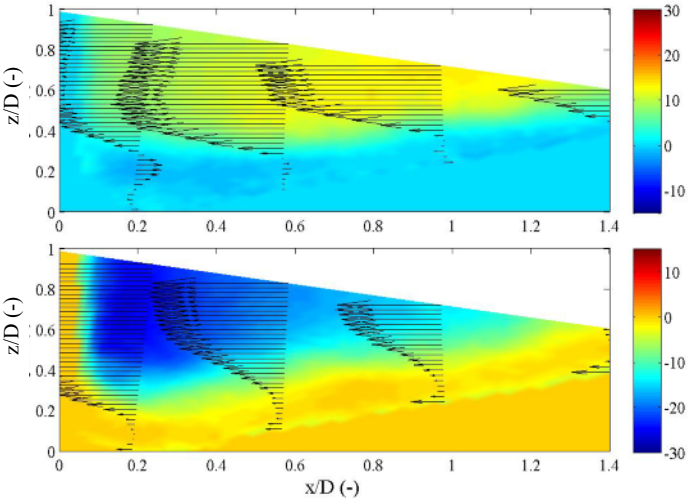

Figure 23 - Time-averaged velocity components in test CC, in the scour hole, at 45º from the symmetry axis. On top: longitudinal component u_p; bottom: vertical component w. Velocities in cm/s.

In Figure 24 the time-averaged vorticity maps for each measuring plane are presented. In the symmetry axis and in the plane at 30º, there seems to occur flow separation in the beginning of the scour hole, wich generates a vortex of different characteristics of the horseshoe vortex observed in fixed bed. Both vortexes have the same sign of vorticity, wich implies the existence of small vortical structures in counter-rotation between them. These can be seen in Figures 27.

Inside the scour hole, near the bed, is noticed the existence of two regions of maximum vorticity. The instantaneous maps show the intermittent behaviour of the horseshoe vortex. Near the cylinder face is observed negative values of vorticity and of higher intensity than what was detected near the bed. This leads to the conclusion that, inside the scour hole, the vorticity generated in the boundary layer which develops along the wall of the cylinder, due the presence of the downflow, is more permanent and relevant than the vorticity generated near the bed.

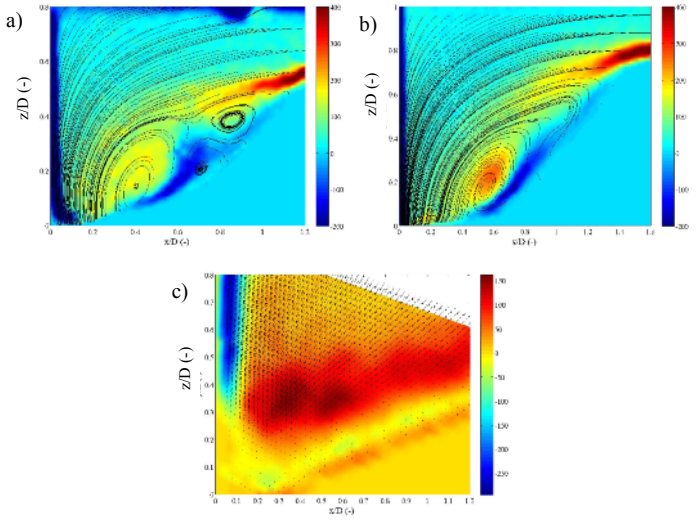

Figure 24 – Time-averaged vorticity maps. Tests CC in a) the vertical plane of symmetry; b) vertical plane at 30º from the symmetry axis; c) the scour hole, at a vertical plane 45º from the symmetry axis.

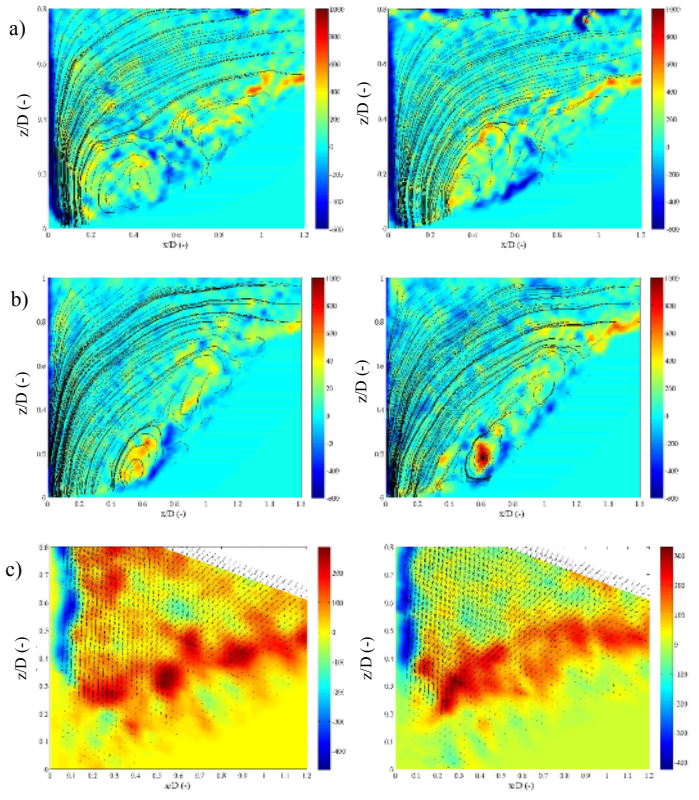

Figure 25 - Instantaneous vorticity maps. Tests CC in a) the vertical plane of symmetry; b) vertical plane at 30º from the symmetry axis; c) the scour hole, at a vertical plane 45º from the symmetry axis.

As a summary, it can said that the down-flow acts as a jet along the wall of the cylinder that, by reaching the flow bed, undergoes separation digging the hole (zone 1) and surrounding the cylinder near the bottom (see Figure 26). Due to this process, the displaced sediments are mostly transported downward, by the downstream flow. A small part is

transported, inside the scour hole, to higher topography levels by the down-flow which incorporates the horseshoe vortex. It was seen that the horseshoe vortex moves frequently towards the cylinder, interacting strongly with the downflow. The bed topography between zones 1 and 2, i.e. the observed cusp, would thus be formed by the upward movement of the jet flow that incorporates the horseshoe vortex and the flow upward from the bottom of the vortex.

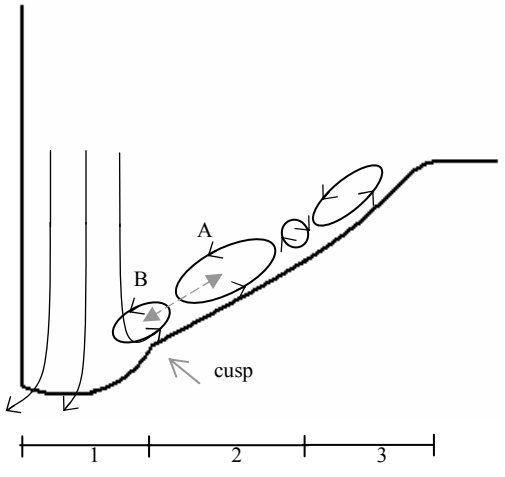

Figure 26. Proposed flow structure in the scour hole in front of the cylindrical pier.

This model is compatible with the proposed by Unger & Hager (2007), but not with those proposed by Qadar (1981) or Muzzammil & Gangadhariah (2003). It follows that the scour mechanism depends fundamentally on the downward flow and not on the intensity of the horseshoe vortex as defended by Shen et al. (1969).

In zone 3, the separate flow is the result of adverse gradient of pressure which results from the sudden deepening of the bed. Among the areas 2 and 3 there are structures in counter-rotation.

6 CONCLUSIONS

The spatial evolution of the flow field in front of a wall-mounted cylinder, placed vertically in a gradually varied flow was investigated by performing experimental tests with a non intrusive method of measurement of flow velocities, the Particle Image Velocimetry (PIV).

The main conclusions of the present work, based on the visualisation and quantification of the flow field in the near field in front of the cylinder, are the following:

- the boundary layer thickness does not influence the intensity of the horseshoe vortex. However, this parameter was seen to govern the dimensions of the equivalent mean-flow vortex.

- the downflow upstream the cylinder plays a major role in the mechanism of local scour near the obstacle. The interaction between the downflow and the horseshoe vortex inside the scour hole leads to the formation of a cusp, separating the region in the scour hole mainly shaped by the down-flow and the region shaped by the horseshoe vortex and the separation vortexes.

Future work should

- investigate the flow pattern inside a scour hole for different stages of development;

- study the influence on the vortex dimensions and intensity of the parameters UD/υ, k_p/D and D_{50}/D;

- investigate the functional relation between D_v/D and I_v/UD as a function of UD/υ for D_{50}/D constant;

- study different values of D/D_{50};

- study, for other values of the parameter k_p/D, the relations between D_v/D and I_v/UD and UD/υ and $U\delta/\upsilon$.

REFERENCES

Baker, C.J. (1979), *The laminar horseshoe vortex*, Journal of Fluid Mechanics 95 (2):347-367.

Baker, C. J. (1980), *The turbulent horseshoe vortex*, Journal of Wind Engineering and Industrial Aerodynamics 6 (1-2):9-23.

Baker, C. J. (1985), *The position of points of maximum and minimum shear stress upstream of cylinders mounted normal to flat plates*, Journal of Wind Engineering and Industrial Aerodynamics 18 (3):263-274.

Dargahi, B. (1989), *The turbulent flow field around a circular cylinder*, Experiments in Fluids 8 (1):1-12.

Ferreira, R. (2005), River Morphodynamics and Sediment Transport. Conceptual Model and Solutions, Tese de Doutoramento, Universidade Técnica de Lisboa, Instituto Superior Técnico, Lisboa.

Graf, W. H. (1998), Fluvial Hydraulics, Wiley, Inglaterra.

Kundu, P; Cohen, I. (2002), Fluid Mechanics, Academic Press, Califórnia.

Morton, B. R. (1987) Trailing vortices in the wakes of surface-mounted obstacles, J. Fluid Mech., 175: 247-293.

Muzzammil, M.; Gangadhariah, T. (2003), The mean characteristics of horseshoe vortex at a cylindrical pier, Journal of Hydraulic Research 41 (3):285-297.

Qadar, A. (1981), The vortex scour mechanism at bridge piers, Proc. ICE Res Theory 71 (3):739-757.

Raudkivi, A. J. (1998) Loose Boundary Hydraulics, A.A. Balkema, Roterdão.

Sahin, B.; Ozturk, N. A.; Akilli, H. (2007), Horseshoe vortex system in the vincinity of the vertical cylinder mounted on flat plate, Flow Measurement and Instrumentation 18:57-68.

Shen, H. W.; Schneider, V. R., Karaki, S. (1969), *Local scour around bridge piers,* Journal of the Hydraulics Division, Proceedings of the American Society of Civil Engineers, Vol. 95, No. HY6, Novembro.

Smart, M. G. (1999), Turbulent Velocity Profiles and Boudary Shear in Gravel Bed Rivers, Journal of Hydraulic Engineering, 125(2):106-117.

Schlichting, H. (1979) Boundary Layer Theory, McGraw-Hill,

Tennekes, H.; Lumley, J. L. (1972) A First Course in Turbulence, The MIT Press.

Unger, J. & Hager, W. (2007) Down-flow and horseshoe vortex characteristics of sediment embedded bridge piers, *Expr. in Fluids*, **42**:1-19.